https://doi.org/10.5194/egusphere-2026-3242
Preprint. Discussion started: 25 June 2026

Fog and low clouds in the Namib Desert may be more resilient than previously thought

Alexandre Mass[1,2], Jan Cermak[1,2], Reto Knutti[3], Anna L. Merrifield[3], and Hendrik Andersen[1,2]

[1]Karlsruhe Institute of Technology (KIT), Institute of Meteorology and Climate Research Atmospheric Trace Gases and Remote Sensing, Karlsruhe, Germany
[2]Karlsruhe Institute of Technology (KIT), Institute of Photogrammetry and Remote Sensing, Karlsruhe, Germany
[3]Institute for Atmospheric and Climate Sciences, ETH Zürich, Zürich, Switzerland

Correspondence: Alexandre Mass (alexandre.mass@kit.edu)

Abstract. Fog and low clouds (FLCs) are essential moisture sources for Namib desert ecosystems. However, their response to climate change remains uncertain because fog processes are not resolved in climate models. Here, we apply a cloud-controlling factor framework in which FLC anomalies are expressed as a linear function of large-scale meteorological drivers, including estimated inversion strength (EIS), relative humidity at 700 hPa (R700), sea surface temperature (SST), and the eastward and northward components of 10 m wind (U10, V10). Sensitivities of FLCs to these drivers are quantified using a statistical model. By applying these sensitivities to projections of the corresponding predictors from CMIP6, we produce the first observationally constrained projections of Namib FLC occurrence. Projected trends remain uncertain and scenario-dependent; however, a robust physical signal emerges. Changes in FLCs are governed by competing influences: SST increase over the southeast Atlantic region reduces FLCs, while increased lower-tropospheric stability as well as circulation changes enhance them. Overall, these results suggest that Namib FLCs may be more resilient to climate change than previously assumed, raising the question of whether similar compensating mechanisms operate in other eastern-ocean boundary-layer upwelling systems, such as those of the Atacama Desert and California.

https://doi.org/10.5194/egusphere-2026-3242
Preprint. Discussion started: 25 June 2026

1 Introduction

Fog is an important source of moisture in the Namib Desert, one of the driest regions on Earth. Despite extremely low rainfall, the region supports diverse ecosystems, many of which depend on fog as a regular water input (Louw and Holm, 1972; Seely and Henschel, 1998; Ebner et al., 2011; Warren-Rhodes et al., 2013; Wang et al., 2019). With projections indicating a general trend of warmer and drier conditions over southern Africa (Maúre et al., 2018; Munday et al., 2025), changes in fog occurrence could have important implications for these ecosystems.

In many regions around the world, fog occurrence has declined in recent decades. This decline has been attributed to reductions of air pollution (Witiw and LaDochy, 2008; Vautard et al., 2009; Fu et al., 2014; Gray et al., 2019), which reduces the availability of cloud condensation nuclei, as well as to rising temperatures that lower relative humidity (Klemm and Lin, 2016; Maurer et al., 2019). In the Namib Desert, however, studies disagree on the sign of fog trends in the observational record: Li et al. (2025) report a decline in fog occurrence, whereas Rohde et al. (2019) infer an increase based on an increase in biomass within the fog belt. Additionally, speculation exists regarding the future evolution of fog in the region, with Mitchell et al. (2020) arguing that a decline appears inevitable. This uncertainty is exacerbated by the difficulty of representing fog in climate models, as the processes governing fog formation occur at spatial scales that are not resolved by these models (Vautard et al., 2009). More broadly, clouds, and low clouds in particular, remain among the most uncertain components of climate simulations (Zelinka et al., 2020; Myers et al., 2021; Bock and Lauer, 2024). For the Namib specifically, only one study has attempted to project fog occurrence using a regional climate model (RCM), and suggests an increase in fog frequency near the coast but a decrease further inland (Haensler et al., 2011). However, the robustness of these fog trends is uncertain because they are based on a single model with biases in present-day fog occurrence.

In the Namib Desert, fog is predominantly of advective nature (Olivier and Stockton, 1989; Seely and Henschel, 1998; Cermak, 2012; Andersen et al., 2019; Spirig et al., 2019; Andersen et al., 2020; Mass et al., 2026). Two main fog types are generally distinguished. Near the coast, fog develops when moist maritime air flows over the cold ocean surface, producing coastal advection fog that is usually limited to a narrow band along the shoreline and influenced by local upwelling cells (Gultepe et al., 2007; Seely and Henschel, 1998; Olivier and Stockton, 1989). Further inland, fog typically results from advected marine stratus clouds whose cloud base reaches the surface, sometimes described as “high fog” (Seely and Henschel, 1998; Malik et al., 2026; Hipler et al., 2026). These events occur mainly between September and March and may penetrate up to 100 km inland (Lancaster et al., 1984; Seely and Henschel, 1998; Andersen et al., 2019). Hereafter, both types are referred to summarily as fog and low clouds (FLCs).

In a prior study, Mass et al. (2026) used a cloud-controlling factor (CCF) framework, typically used to assess cloud feedbacks (Klein et al., 2018), to quantify FLC sensitivities to large-scale meteorological controls in two fog-prone regions of the Namib Desert. Building on this framework, we combine observationally derived FLC sensitivities with projected changes in the controlling factors from selected GCMs of the Coupled Model Intercomparison Project Phase 6 data (CMIP6; Eyring et al., 2016) to provide the first observationally-constrained estimates of future changes in Namib FLCs. Based on the observational sensitivities, we hypothesize that future SST warming over the southeast Atlantic region will decrease FLC cover, while increased

https://doi.org/10.5194/egusphere-2026-3242
Preprint. Discussion started: 25 June 2026

lower-tropospheric stability and changes in coastal circulation may offset this response, leading to competing influences on FLCs under climate change.

2 Results and discussion

2.1 Projected changes in Namib FLCs

Detrended and deseasonalized anomalies are used in a ridge regression framework to estimate spatial sensitivity patterns at a resolution of 1.25° latitude × 1.875° longitude (see Sections A2 and A3 for details). Reanalysis fields of cloud-controlling factors are taken from two reanalysis datasets (ERA5 and MERRA-2) across two fog hotspots in the Namib Desert: the Central Namib (CN; 22°S–24°S) and the Angolan Namib (AN; 15°S–17°S), resulting in four setups. Outputs from five CMIP6 models are then applied under the low- and high-forcing shared socioeconomic pathways, SSP126 and SSP585 (O'Neill et al., 2017), to capture the full range of projected responses. Projected FLC cover anomalies for 2015–2100 are shown in Figure 1 as 5-year rolling means. The four panels correspond to AN-ERA5 (Fig. 1a), CN-ERA5 (Fig. 1b), AN-MERRA-2 (Fig. 1c), and CN-MERRA-2 (Fig. 1d). The green and purple lines represent SSP126 and SSP585, the weakest and strongest forcing scenarios, respectively, and the shaded areas indicate the total uncertainty.

Under SSP126, projected FLC trends are weak across all configurations, as indicated by the dashed lines. In the AN, FLC trends are small, with statistically significant decrease in the MERRA-2-based setup (AN-MERRA-2: $-0.09\,\% \cdot \mathrm{decade}^{-1}$). In the CN, trends are also weak, with a statistically significant decrease in the ERA5-based setup (CN-ERA5: $-0.06\,\% \cdot \mathrm{decade}^{-1}$). These weak trends mirror the near-zero trends in FLC anomalies observed for 1982–2019 in Mass et al. (2026), suggesting that changes in FLC drivers are either too weak or offset each other.

Under SSP585, projected FLC trends are more pronounced. In the CN, both configurations project increasing FLC cover, with positive and statistically significant trends in CN-ERA5 ($+0.10\,\% \cdot \mathrm{decade}^{-1}$) and CN-MERRA-2 ($+0.26\,\% \cdot \mathrm{decade}^{-1}$). A similar positive trend is found for AN-ERA5 ($+0.27\,\% \cdot \mathrm{decade}^{-1}$). These positive trends are consistent with the results of Haensler et al. (2011), the only other study that has examined future projections of fog in the Namib Desert, which reported increasing coastal fog occurrence using the REMO regional climate model (Jacob, 2001). In contrast, the AN-MERRA-2 configuration shows a trend of the opposite sign at $-0.30\,\% \cdot \mathrm{decade}^{-1}$.

This difference is further illustrated by the SSP585 mean FLC cover anomaly for 2080–2100 for each individual model, shown as purple symbols in Fig. 1. In all configurations, FGOALS-f3-L exhibits strong positive FLC cover anomalies. The remaining models show weaker but generally positive FLC anomalies, except in the AN–MERRA-2 configuration. In this case, FGOALS-f3-L still exhibits a positive FLC anomaly, although with a smaller magnitude, while the other four exhibit reduced FLC cover anomalies of around 3% during the 2080–2100 period. A similar pattern is evident for SSP126 (green), with FGOALS-f3-L consistently exhibiting positive FLC anomalies, whereas the remaining models lie closer to zero and are generally negative; the intermodel spread is also smaller than in SSP585.

This spread across GCMs partly arises from the ClimSIPS model selection algorithm (see Section A2), which maximizes the range of projected temperature and precipitation changes across the WSAF region (Iturbide et al., 2020) within the ensemble.

https://doi.org/10.5194/egusphere-2026-3242
Preprint. Discussion started: 25 June 2026

The resulting uncertainty $\sigma_{\text{gcm}}(t)$ represents one component of the total uncertainty. A second source arises from the estimation of ridge regression coefficients ($\sigma_{\text{stat}}(t)$). For each setup, the total uncertainty is obtained as the sum in quadrature of these components (see Section A4 for more details) and is shown by the shaded areas in Figure 1. The total uncertainty remains approximately constant for SSP126, whereas it increases over time for SSP585. This increase is driven by $\sigma_{\text{stat}}(t)$, which grows with time under increasing forcing, while $\sigma_{\text{gcm}}(t)$ remains relatively constant, reflecting stable model spread. This is illustrated in Figure A2, which shows the fractional contributions of $\sigma_{\text{stat}}(t)$ and $\sigma_{\text{gcm}}(t)$ to the total variance for each setup. In 2015, $\sigma_{\text{stat}}(t)$ accounts for approximately 10% of the total variance across all configurations. By the end of the century, this fraction increases to 25% under SSP126 and to 80% under SSP585. Moreover, for each CMIP6 model, all available ensemble members are averaged together. The resulting projections therefore primarily estimate the forced trend and do not fully sample internal variability. Treating ensemble members separately would broaden the projected uncertainty range.

In addition to the total uncertainty, changing the reanalysis dataset leads to opposite trends in the AN region, despite overlapping uncertainty ranges. As only two reanalyses are considered, this difference is not interpreted as a distinct source of uncertainty but rather as a sensitivity to the choice of the reanalysis dataset, illustrating how different datasets can lead to "uncertain situations" in the interpretation of climate trends (Simpson et al., 2025). These opposite trends arise from differences in the SST coefficient maps (not shown). Despite a strong spatial correlation (0.95) between ERA5 and MERRA2 in the AN region (see Table A1), SST changes in the GCM projections are substantially larger than those of the other predictors, reaching up to six times the historical standard deviation under SSP585, whereas the other predictors rarely exceed two standard deviations (not shown). As a result, small differences in SST sensitivities between ERA5 and MERRA2 are strongly amplified and can reverse the sign of the projected trends.

The large total uncertainty and the sensitivity to the choice of reanalysis highlight important limitations of the projections. However, rather than providing forecasts of future FLC changes, these projections offer a framework to explore how changes in the predictors translate into FLC variability. The next section therefore examines the contributions of individual predictors to the projected trends.

https://doi.org/10.5194/egusphere-2026-3242
Preprint. Discussion started: 25 June 2026

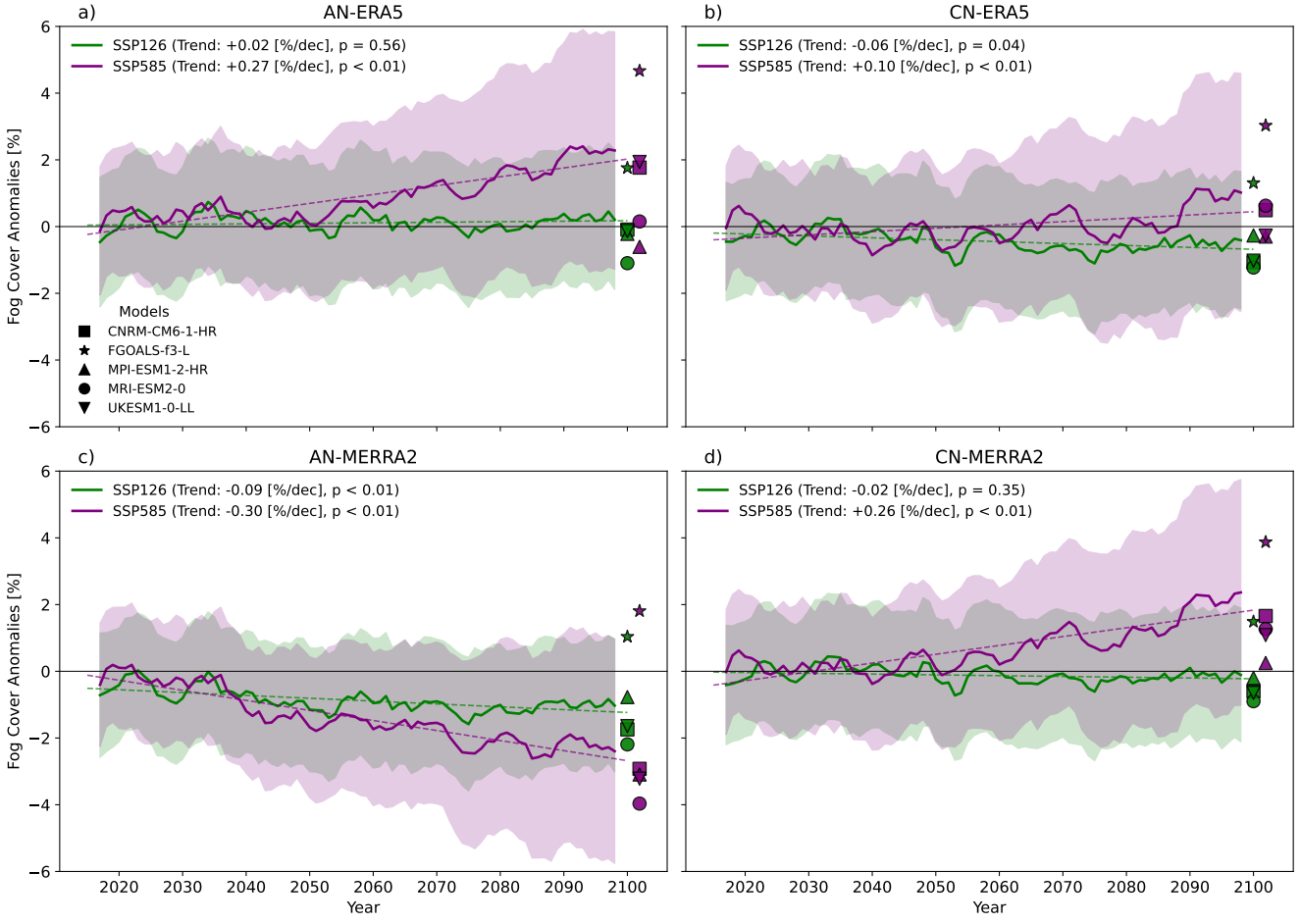

Figure 1. Projected changes in FLC cover anomalies (%) for 2015–2100. Solid lines show the 5-year rolling mean of the ensemble mean of five CMIP6 models for the Angolan Namib (AN) and Central Namib (CN), based on sensitivities derived from ERA5 and MERRA-2: **a)** AN-ERA5, **b)** CN-ERA5, **c)** AN-MERRA-2, and **d)** CN-MERRA-2. Purple and green lines denote SSP585 and SSP126, respectively, and shading indicates total uncertainty. Dashed lines indicate the corresponding linear trends. Symbols at the end of each panel show the mean FLC cover anomaly of each model for 2080–2100 under SSP126 in green and SSP585 in purple.

2.2 Drivers of projected FLC changes

In Figure 2, the projected FLC cover anomaly trends presented in Section 2.1 are decomposed into contributions from each
105 predictor for each model and SSP scenario: SSP126 (green), SSP370 (blue), and SSP585 (purple). The main result is that the opposing contributions of EIS, R700, U10, and V10 versus SST identified under present-day climate conditions (Mass et al., 2026) persist in future projections, indicating resilience of the system to climatic changes. The signs of the predictor trend contributions are consistent with the projected changes in the corresponding drivers in the GCM ensemble mean (see Fig. 3) when combined with the sensitivities derived from the present-day climate (see Fig. A1). Increased boundary-layer stability

https://doi.org/10.5194/egusphere-2026-3242
Preprint. Discussion started: 25 June 2026

(Fig. 3a) favors the persistence of FLCs by suppressing mixing across the inversion (Bretherton et al., 2013; Myers and Norris, 2016; Scott et al., 2020; Ceppi and Nowack, 2021). A drier free troposphere (Fig. 3b) can further enhance cloud-top radiative cooling and support low-cloud development in the region (Christensen et al., 2013; Andersen et al., 2020). In contrast, SST warming (Fig. 3c) tends to reduce the thermal contrast between the ocean surface and the overlying air masses responsible for FLC formation (Olivier and Stockton, 1989; Cermak, 2012; Spirig et al., 2019; Andersen et al., 2020). Circulation changes (Fig. 3d and e) indicate an increase in the onshore advection of the marine boundary layer air masses in which FLCs are formed (Andersen et al., 2020). Such an enhanced onshore circulation is already observed over the recent decades and can be understood as a consequence of an intensified thermal wind associated with warming over the southern African continent (Attwood et al., 2024; Tatro and Zuidema, 2025).

By grouping the predictors into thermodynamic (EIS, R700, and SST) and circulation (U10 and V10) contributions, and excluding FGOALS-f3-L due to its anomalously weak SST warming, it becomes apparent that thermodynamic trend contributions are mostly negative, consistent with the observed global fog decline (Vautard et al., 2009; Klemm and Lin, 2016). In contrast, changes in circulation counteract this effect, making FLCs more resilient to climate change. This raises the question of whether similar mechanisms may operate in other eastern boundary upwelling systems, where onshore advection of marine boundary layer clouds dominate, potentially enhancing FLC resilience there as well.

The relative importance of these opposing contributions determines the resulting FLC trends under the different forcing scenarios. Under the lowest forcing scenario, SSP126, these opposing influences are generally small and largely compensate each other, leading to total trends close to zero. Under stronger forcing scenarios such as SSP370 and SSP585, the total trends and model spread depend primarily on the magnitude of the negative SST contribution. Weaker SST contributions lead to positive trends in AN-ERA5, CN-ERA5, and CN-MERRA-2 (Fig. 2a,b,d), whereas a stronger SST contribution results in a negative trend for AN-MERRA-2 (Fig. 2c). Additionally, for a given model, the partial contributions scale monotonically with the magnitude of the forcing, suggesting that stronger climate forcing primarily amplify the same underlying processes.

However, substantial variability remains between models. This variability arises primarily from differences in the magnitude of the SST contributions, which largely determine the sign of the projected FLC trends. While the contributions from EIS, R700, and the wind components are generally consistent across models, SST responses vary more strongly in magnitude, leading to larger inter-model differences in the total projected trends. For example, UKESM1-0-LL features a relatively strong negative SST contribution across all four setups, whereas FGOALS-f3-L exhibits weaker negative contributions, or even positive ones in CN-MERRA-2, in contrast to the other models.

The inter-model variability in SST projections is a well-known feature of the CMIP6 ensemble (Masson-Delmotte et al., 2021). This spread partly arises from models with higher equilibrium climate sensitivity than in CMIP5 (Taylor et al., 2012), largely driven by differences in cloud–climate feedbacks that vary substantially across models and influence the magnitude of surface warming (Meehl et al., 2020; Zelinka et al., 2020). In addition, differences in the efficiency of ocean heat uptake, related to the representation of vertical mixing and thermodynamic processes within the ocean interior, contribute to variations in the projected SST response among models (Gregory, 2000; Huber and Zanna, 2017).

In the Benguela upwelling system, recent studies indicate a southward displacement of the coastal upwelling system under

https://doi.org/10.5194/egusphere-2026-3242
Preprint. Discussion started: 25 June 2026

both recent climate variability and projected future climate change (Abrahams et al., 2021; Bordbar et al., 2023; Gallego et al., 2025). Such a spatial shift would likely modify the SST sensitivity pattern, although this is beyond the scope of the present analysis.

Overall, despite the substantial inter-model variability in SST trends and potential shifts in coastal upwelling patterns, the balance between the different drivers controlling FLC variability remains robust, suggesting that circulation changes could make the coastal fog system more resilient than expected from the forced thermodynamic response alone.

https://doi.org/10.5194/egusphere-2026-3242
Preprint. Discussion started: 25 June 2026

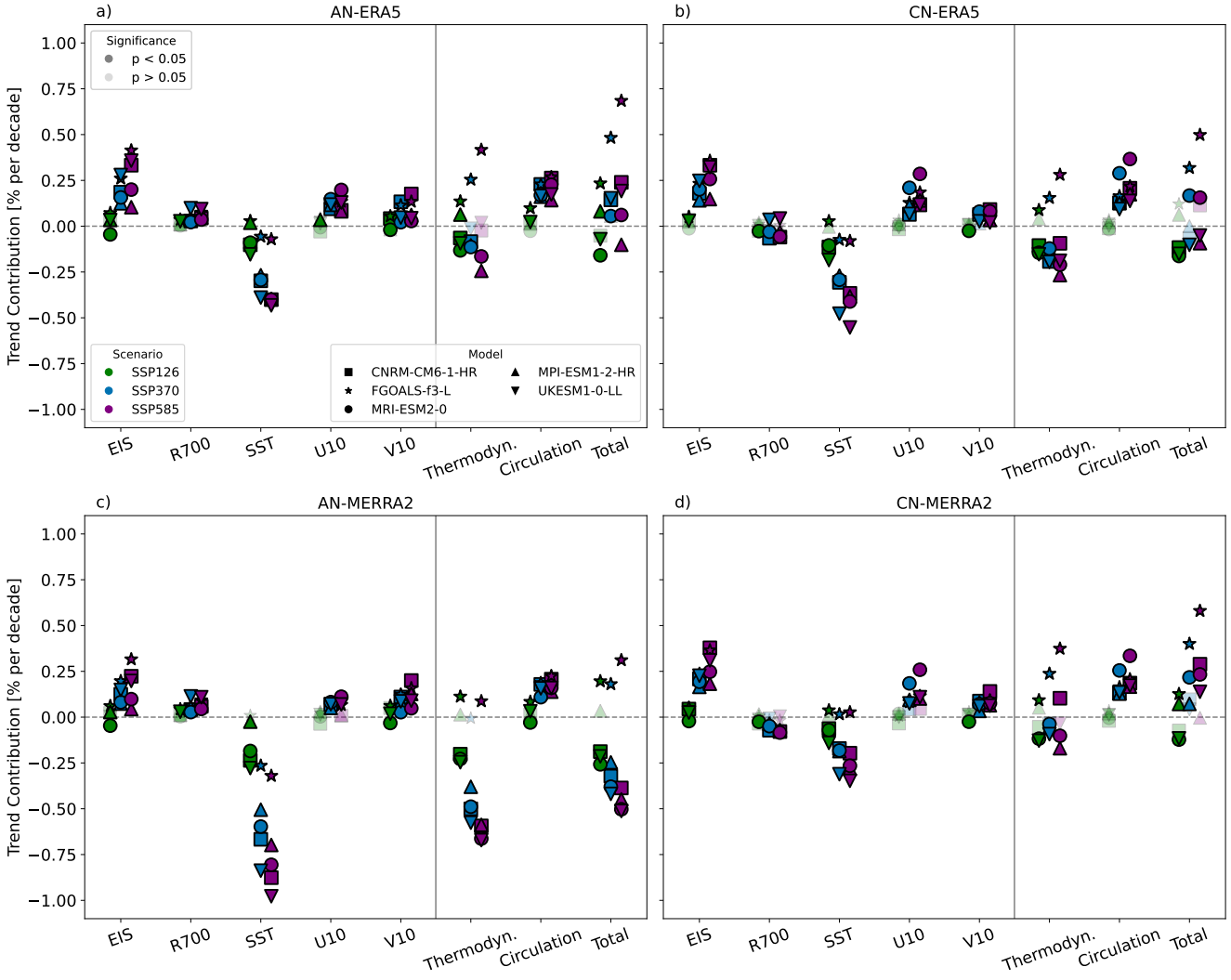

Figure 2. Partial trend contributions to FLC cover anomalies (%) for 2015–2100 from each predictor (EIS, R700, SST, U10, V10). Aggregated Thermodynamic (EIS + R700 + SST), Circulation (U10 + V10), and Total contributions are also shown. Panels show the Angolan Namib (AN) and Central Namib (CN) based on sensitivities derived from ERA5 and MERRA-2: **a)** AN-ERA5, **b)** CN-ERA5, **c)** AN-MERRA-2, and **d)** CN-MERRA-2. Colors denote the different Shared Socio-economic Pathways (SSPs): SSP126 (green), SSP370 (blue), and SSP585 (purple). Individual GCMs are shown as symbols. Statistically significant trend contributions ($p < 0.05$) are shown as solid markers, while non-significant contributions are shown with transparent markers.

https://doi.org/10.5194/egusphere-2026-3242
Preprint. Discussion started: 25 June 2026

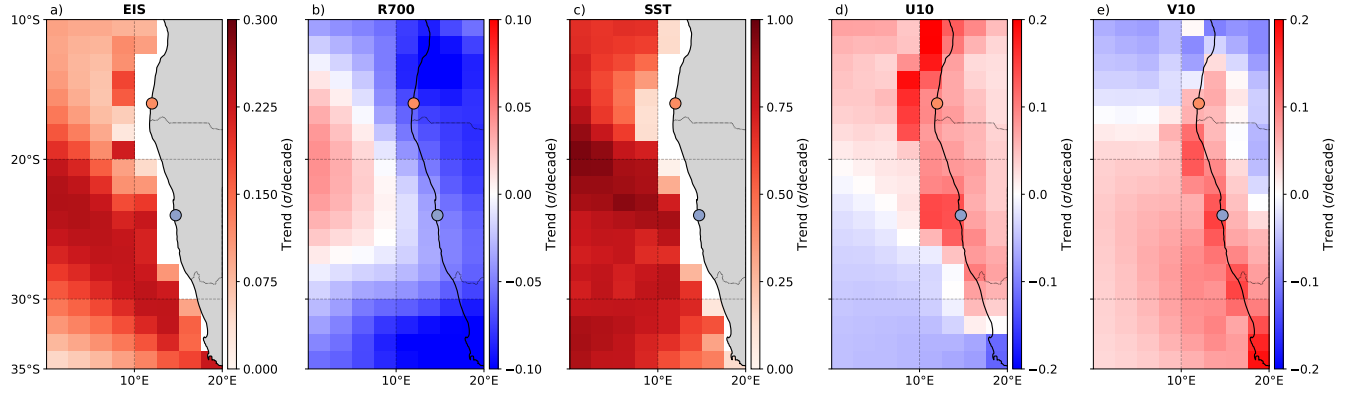

Figure 3. Ensemble mean decadal trends [$\sigma \cdot \mathrm{decade}^{-1}$] for 2015–2100 in the predictors: **a)** EIS, **b)** R700, **c)** SST, **d)** U10, and **e)** V10. The centers of the Angolan Namib (AN) and Central Namib (CN) are indicated by the orange and blue circles, respectively. White regions near the coastline for EIS and SST are the result of the common land mask.

3 Conclusions

Fog and low clouds (FLCs) are key components of the Namib Desert climate, yet their future evolution remains difficult to assess because fog formation occurs at spatial scales that are not resolved in global climate models (Vautard et al., 2009). To address this limitation, we used a cloud-controlling factor (CCF) framework (Klein et al., 2018) to estimate sensitivities of FLC anomalies to large-scale meteorological drivers based on the present-day climate. These sensitivities were then combined with projected changes in the drivers from CMIP6 simulations to estimate projections of FLC cover anomalies in two fog-prone regions of the Namib: the Angolan Namib (AN) and the Central Namib (CN) (Andersen and Cermak, 2018).

This approach has limitations. The results depend first on the sensitivities derived from reanalysis data, which differ slightly depending on whether they are derived from ERA5 or MERRA-2. In addition, the projected changes in the predictors, particularly SST, vary substantially across CMIP6 models. This is partly intentional and reflects the aim of capturing a broad range of climatic changes across the GCM ensemble. Together, these statistical and GCM uncertainties lead to a range of possible FLC projections. The projections should therefore not be interpreted as deterministic forecasts, but as a framework for exploring the underlying processes.

Within this framework, future changes in Namib FLC cover anomalies appear to be governed by competing influences among the large-scale drivers. Increases in atmospheric stability favor FLCs, whereas SST warming suppresses them, consistent with the low-cloud feedback (Myers and Norris, 2016; Andersen et al., 2020; Scott et al., 2020; Ceppi and Nowack, 2021; Wu et al., 2025). Additionally, projected circulation changes associated with intensified thermal winds enhance onshore advection and thereby favor FLCs in the Namib Desert. This suggests a certain resilience of Namib fog to climate warming relative to other marine low-cloud systems, raising the question of whether similar circulation-driven resilience may also occur in fog systems such as those of the Atacama Desert or California..

These results highlight the importance of improving projections of regional SST patterns in eastern boundary upwelling sys-

https://doi.org/10.5194/egusphere-2026-3242
Preprint. Discussion started: 25 June 2026

tems, as SST exhibits the largest projected changes (Wang et al., 2015) among the drivers considered and therefore plays a key role in shaping future FLC variability. Accurately representing future SST patterns in these regions remains critical (Zuidema et al., 2016) for anticipating changes in fog and low clouds along the Namibian coast. Future work could extend this approach by allowing spatially evolving fog regions, thereby capturing potential shifts in the geographical distribution of fog and low clouds along the Namibian coast.

Appendix A: Data and methods

A1 Satellite-based FLC cover

FLC cover is derived from the satellite-based detection algorithm introduced by Andersen and Cermak (2018). The algorithm uses observations from the Spinning Enhanced Visible and Infrared Imager (SEVIRI) onboard the Meteosat Second Generation (MSG) satellites, which provide imagery at 3 km spatial resolution and 15 min temporal resolution (Schmetz et al., 2002). By combining infrared measurements with threshold-based and image-analysis techniques, the algorithm identifies FLC occurrence consistently throughout the diurnal cycle.

The algorithm produces a binary field of FLC occurrence for each grid cell at 15-minute intervals. Evaluation with in situ observations demonstrates good performance, with a probability of detection of 94% and an overall classification accuracy of 97%. From these data, a FLC cover metric is calculated as the relative frequency of FLC occurrence over a 24-hour period starting at 12:00 UTC (FLC occurrence peaks at night and early morning), in a chosen region, following Mass et al. (2026). From daily average FLC cover, a monthly mean FLC cover is then calculated for the analysis period 2004–2019. Two regional fog hotspots in the Namib Desert are considered: the Angolan Namib (AN; 15°S–17°S) and the Central Namib (CN; 22°S–24°S). These regions correspond to two fog-prone coastal sectors of the Namib Desert (Andersen and Cermak, 2018; Mass et al., 2025, 2026). To improve the signal to noise ratio and because FLC occurrence decreases inland, the analysis is restricted to grid cells located within 25 km of the coastline. This spatially averaged, deseasonalized, and detrended monthly FLC cover serves as the predictand in the statistical model.

A2 Global climate model selection

GCMs are selected using the Climate Model Selection by Independence, Performance, and Spread (ClimSIPS) framework (Merrifield et al., 2023). This method ranks climate models according to their historical performance, their independence from other models, and their contribution to ensemble spread. Model independence is considered because many climate models share components or development lineages, leading to genealogical relationships within the CMIP ensemble rather than fully independent realizations (Knutti et al., 2013). In this study, model performance is evaluated using SST climatologies from ERA5 (Hersbach et al., 2020) over the Benguela region (5°W–35°E, 40°S–0°) for annual, DJF, and JJA means during 1995–2014, together with annual mean shortwave cloud radiative effect (SWCRE) fields for 2001–2018 from the Clouds and the Earth's Radiant Energy System (CERES) Energy Balanced and Filled surface flux products (Loeb et al., 2018; Loeb and Doelling,

https://doi.org/10.5194/egusphere-2026-3242
Preprint. Discussion started: 25 June 2026

2020). SST is included because it exhibits substantial variability across CMIP6 models (Masson-Delmotte et al., 2021) and constitutes a key driver of fog and low cloud variability along the Namibian coast (Mass et al., 2026), while SWCRE provides an observational constraint on the radiative effects of fog and low clouds. The spread criterion is based on projected changes in near-surface air temperature (tas) and precipitation (pr) over the WSAF region (Iturbide et al., 2020), computed as the difference between the 2070–2099 and 1995–2014 climatological means, thereby capturing a broad range of climatic changes across the GCM ensemble. Based on ClimSIPS, the following CMIP6 models were selected for the analysis: FGOALS-f3-L (He et al., 2019), CNRM-CM6-1-HR (Voldoire et al., 2019), UKESM1-0-LL (Sellar et al., 2019), IPSL-CM6A-LR (Boucher et al., 2020), and MPI-ESM1-2-HR (Mauritsen et al., 2019). For each selected CMIP6 model, all available ensemble members are averaged to reduce the influence of internal variability. To ensure spatial consistency across models, all predictor fields were regridded to a common grid corresponding to the lowest native resolution among the selected models, here taken as the UKESM1-0-LL atmospheric grid (1.25° latitude × 1.875° longitude). The regridding was performed using bilinear interpolation. This approach preserves the large-scale spatial patterns of the predictors while enabling a consistent comparison across models.

To reduce systematic differences between reanalysis predictors and GCM simulations, a simple variance scaling bias correction is applied (Teutschbein and Seibert, 2012). Scaling factors are derived from the present-day climate using ERA5 or MERRA-2 (Gelaro et al., 2017) predictor fields and subsequently applied to the corresponding GCM predictors. This approach adjusts the mean and standard deviation of the predictors while preserving the relationships between them. More advanced bias-correction methods such as quantile mapping are not used, as univariate bias correction can modify the multivariate relationships between predictors (Maraun, 2016) required by the ridge regression framework employed in this study (see below).

A3 Cloud-controlling factor analysis framework

The statistical framework used in this study follows the cloud-controlling factor (CCF) approach described in detail in Mass et al. (2026). In this framework, anomalies in fog and low cloud (FLC) cover are related to anomalies in a set of large-scale environmental drivers commonly used to study marine low clouds (Klein et al., 2018; Scott et al., 2020; Ceppi and Nowack, 2021; Andersen et al., 2022, 2023; Ceppi et al., 2025). The predictors considered here are the estimated inversion strength (EIS), computed following the method developed by Wood and Bretherton (2006); relative humidity at 700 hPa (R700); sea surface temperature (SST); and the eastward and northward components of the near-surface wind (U10 and V10).

FLC cover anomalies are averaged over the AN and CN regions, while the predictor fields are considered over a larger surrounding domain covering 10°S–35°S and 5°E–20°E, corresponding to a 25° latitude × 15° longitude region. Following earlier CCF studies (Ceppi and Nowack, 2021; Ceppi et al., 2025; Andersen et al., 2023; Wilson Kemsley et al., 2024), large-scale predictor fields from the surrounding domain are related to a regional predictand, rather than relying on local grid-point-wise relationships. The domain was selected to capture most of the synoptic-scale variability of the relevant meteorological fields (Andersen et al., 2020; Mass et al., 2025) and to encompass the regions of interest. This choice ensures that large-scale circulation patterns and non-local influences, such as coastal upwelling cells, are represented and that SST anomalies can be related

https://doi.org/10.5194/egusphere-2026-3242
Preprint. Discussion started: 25 June 2026

to FLC variability over land. Because ridge regression regularizes the predictor coefficients (see below), the results are not expected to be highly sensitive to modest changes in domain size, provided that the main spatial features are included. The final spatial extent therefore reflects a compromise between encompassing the regions relevant for FLC processes and limiting the domain size to avoid excessive regularization.

Two predictor sets are constructed to improve robustness: one based on ERA5 meteorological fields combined with NOAA OI SST (Huang et al., 2021), and another based on MERRA-2 meteorological fields combined with the same SST dataset. This results in four configurations: AN–ERA5, CN–ERA5, AN–MERRA-2, and CN–MERRA-2. All predictor fields are subsequently interpolated onto the UKESM1-0-LL atmospheric grid (1.25° latitude × 1.875° longitude) using bilinear interpolation so that they can be used consistently together with the GCM predictor fields.

The sensitivities of FLC cover anomalies to the predictor anomalies are estimated using ridge regression (Hoerl and Kennard, 1970). In this setup, the regional FLC anomaly is modeled as a linear combination of the spatial predictor anomalies across the domain. Ridge regression is well suited for this study for two important reasons. First, it performs well in cases with many collinear predictors (Bishop and Nasrabadi, 2006; Dormann et al., 2013). Second, the number of predictors is large relative to the number of observations, which increases the risk of overfitting. Ridge regression is an extension of linear regression where the cost function additionally features an l^2-norm regularization term that penalizes large regression coefficients, controlled by the regularization parameter $\lambda(r)$. By shrinking the coefficients, the regularization limits the tendency of the model to fit noise in the training data. The value of $\lambda(r)$ determines the balance between model flexibility and regularization: small values allow a more flexible model that may be prone to overfitting, whereas large values impose stronger regularization and can increase model bias.

It is important to emphasize that the regression captures statistical associations between the predictors and FLC cover rather than direct causal links. The resulting sensitivity patterns should therefore be interpreted as indicators of the relative predictive influence of the different drivers within the synoptic variability of the region.

The resulting sensitivity patterns are shown in Fig. A1 for the AN–ERA5 configuration, while a detailed discussion of these patterns at higher spatial resolution is provided in Mass et al. (2026). Table A1 summarizes the spatial correlations between the sensitivities derived from the ERA5- and MERRA-2-based predictor sets, indicating good agreement across configurations.

Projected FLC cover anomalies are estimated by combining these sensitivities with ensemble-mean GCM changes in the predictors. Specifically, the projected FLC cover anomaly is calculated as the scalar product between the estimated sensitivities and the projected predictor anomalies. This approach relies on the stationarity assumption that the relationships between FLC cover and the controlling factors derived in the present-day climate remain valid under future climate conditions.

https://doi.org/10.5194/egusphere-2026-3242
Preprint. Discussion started: 25 June 2026

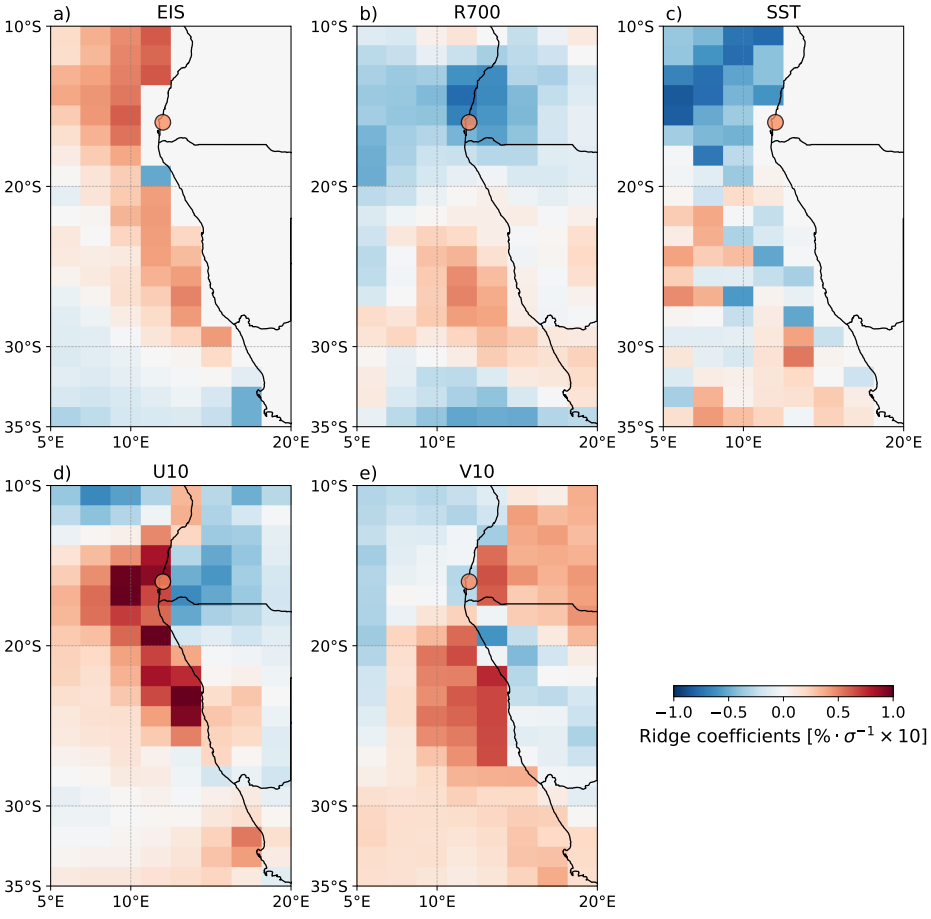

Figure A1. Sensitivities fields [% × standard deviation], for each predictor in the AN-ERA5 configuration: **(a)** estimated inversion strength (EIS), **(b)** relative humidity at 700 hPa (R700), **(c)** sea surface temperature (SST), **(d)** 10 m eastward wind (U10), and **(e)** 10 m northward wind (V10). The orange circle indicates the center of the AN region.

Table A1. Spatial correlations (Pearson's r) between the sensitivity patterns derived from the ERA5 and MERRA-2 predictor sets.

predictor	CN	AN
EIS	0.77	0.69
R700	0.71	0.68
SST	0.96	0.95
U10	0.73	0.73
V10	0.67	0.67

https://doi.org/10.5194/egusphere-2026-3242
Preprint. Discussion started: 25 June 2026

A4 Uncertainty

For each configuration, uncertainty in projections of FLC cover anomalies arises from ridge regression coefficient estimation, referred to as statistical uncertainty, and from inter-model spread, referred to as GCM uncertainty.

To quantify GCM uncertainty, the trained ridge regression model is applied to each climate model, producing a set of projections across the CMIP6 ensemble. The GCM uncertainty is defined as the standard deviation of these projections across models, denoted as $\sigma_{\mathrm{gcm}}(t)$.

Statistical uncertainty is estimated using a moving block bootstrap (Lahiri, 2003). Autocorrelation analysis indicates that temporal dependence is relevant at timescales shorter than 6 months. Therefore, a block length of 6 months is used to preserve within-block dependence while treating blocks as approximately independent. A total of 500 bootstrap realizations are generated by resampling blocks with replacement. The statistical uncertainty is defined as the standard deviation across bootstrap realizations, denoted as $\sigma_{\mathrm{stat}}(t)$.

Assuming independence between both sources of uncertainty, the total uncertainty is computed as:

$$\sigma_{\mathrm{total}}(t) = \sqrt{\sigma^2_{\mathrm{stat}}(t) + \sigma^2_{\mathrm{gcm}}(t)}. \tag{A1}$$

The relative contribution of each source is quantified using fractional contributions:

$$f_{\mathrm{stat}}(t) = \frac{\sigma^2_{\mathrm{stat}}(t)}{\sigma^2_{\mathrm{stat}}(t) + \sigma^2_{\mathrm{gcm}}(t)}, \quad f_{\mathrm{gcm}}(t) = \frac{\sigma^2_{\mathrm{gcm}}(t)}{\sigma^2_{\mathrm{stat}}(t) + \sigma^2_{\mathrm{gcm}}(t)}. \tag{A2}$$

Changes in the fractional contributions over time, highlighting the relative importance of each uncertainty source across configurations and scenarios, are shown in Fig. A2.

https://doi.org/10.5194/egusphere-2026-3242
Preprint. Discussion started: 25 June 2026

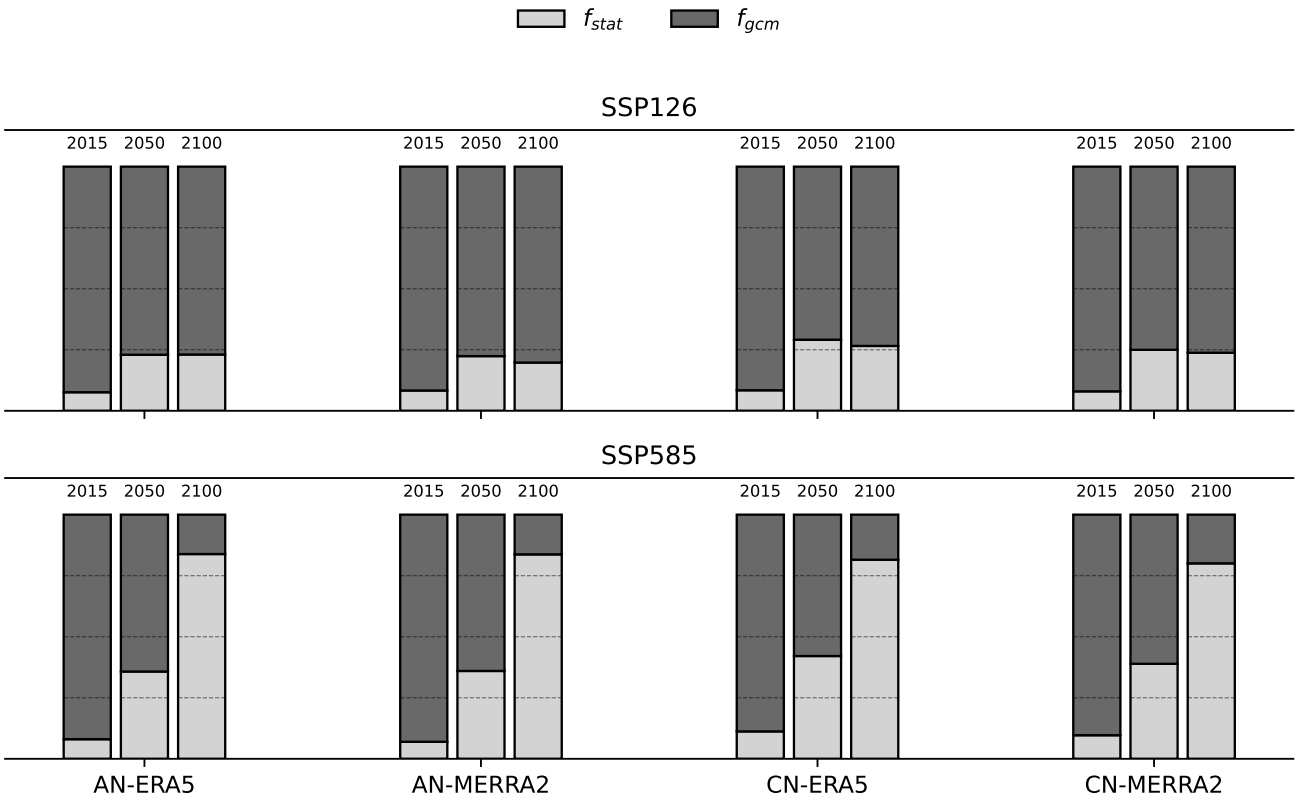

Figure A2. Changes in the fractional contributions of statistical (f_{stat}) and GCM (f_{gcm}) uncertainty to the total variance of FLC cover anomaly projections, evaluated at selected years (2015, 2050, 2100) for different configurations (AN-ERA5, AN-MERRA2, CN-ERA5, CN-MERRA2) and scenarios (SSP126 and SSP585).

Code and data availability. ERA5 data were obtained from the Copernicus Climate Change Service via the Climate Data Store (https://cds.climate.copernicus.eu/). MERRA-2 data were provided by the Goddard Space Flight Center Distributed Active Archive Center (GSFC DAAC; https://daac.gsfc.nasa.gov/). The following data collections were used: Global Modeling and Assimilation Office and Pawson (2015a, b, c). NOAA OI SST V2 High Resolution Dataset data were provided by the NOAA PSL, Boulder, Colorado, USA, from their website at https://psl.noaa.gov. CMIP6 data are available through the Earth System Grid Federation (ESGF; https://esgf.github.io/index.html). Satellite FLC data are available at https://radar.kit.edu/radar/de/dataset/pebssmnzn7n8czg5 (DOI: 10.35097/pebssmnzn7n8czg5). Code for data processing is available from the corresponding author upon reasonable request.

https://doi.org/10.5194/egusphere-2026-3242
Preprint. Discussion started: 25 June 2026

Author contributions. AM, HA, and JC had the idea for the analysis. AM obtained and analyzed the datasets, conducted the original research, and wrote the manuscript. ALM contributed to model selection through the application of the ClimSIPS framework. JC, RK, ALM and HA contributed to the interpretation of the findings and the preparation of the manuscript.

Competing interests. HA is guest editor for the inter-journal (ACP/AMT/AR/ESSD) Special Issue "Aerosol, fog, climate, and biogeochemistry in southern Africa". The remaining authors declare that they have no conflicts of interest.

Acknowledgements. Funding for this study was provided by Deutsche Forschungsgemeinschaft (DFG) in the project Namib Fog Life Cycle Analysis - Aerosols and Climate (NaFoLi[CA]^2), project number 462604610. AM gratefully acknowledges funding from the Graduate School for Climate and Environment (GRACE), which supported a research stay at ETH Zürich and facilitated collaboration with ALM and RK. We thank Paquita Zuidema and Erich Fischer for discussion and ideas which improved the study.

https://doi.org/10.5194/egusphere-2026-3242
Preprint. Discussion started: 25 June 2026

References

Abrahams, A., Schlegel, R. W., and Smit, A. J.: Variation and change of upwelling dynamics detected in the world's eastern boundary upwelling systems, Frontiers in Marine Science, 8, 626 411, https://doi.org/10.3389/fmars.2021.626411, 2021.

Andersen, H. and Cermak, J.: First fully diurnal fog and low cloud satellite detection reveals life cycle in the Namib, Atmospheric Measurement Techniques, 11, 5461–5470, https://doi.org/10.5194/amt-11-5461-2018, 2018.

Andersen, H., Cermak, J., Solodovnik, I., Lelli, L., and Vogt, R.: Spatiotemporal dynamics of fog and low clouds in the Namib unveiled with ground- and space-based observations, Atmospheric Chemistry and Physics, 19, 4383–4392, https://doi.org/10.5194/acp-19-4383-2019, 2019.

Andersen, H., Cermak, J., Fuchs, J., Knippertz, P., Gaetani, M., Quinting, J., Sippel, S., and Vogt, R.: Synoptic-scale controls of fog and low-cloud variability in the Namib Desert, Atmospheric Chemistry and Physics, 20, 3415–3438, https://doi.org/10.5194/acp-20-3415-2020, 2020.

Andersen, H., Cermak, J., Zipfel, L., and Myers, T. A.: Attribution of observed recent decrease in low clouds over the Northeastern Pacific to cloud-controlling factors, Geophysical Research Letters, 49, e2021GL096 498, https://doi.org/10.1029/2021GL096498, 2022.

Andersen, H., Cermak, J., Douglas, A., Myers, T. A., Nowack, P., Stier, P., Wall, C. J., and Wilson Kemsley, S.: Sensitivities of cloud radiative effects to large-scale meteorology and aerosols from global observations, Atmospheric Chemistry and Physics, 23, 10 775–10 794, https://doi.org/10.5194/acp-23-10775-2023, 2023.

Attwood, K., Washington, R., and Munday, C.: The Southern African Heat Low: Structure, Seasonal and Diurnal Variability, and Climatological Trends, Journal of Climate, 37, 3037 – 3053, https://doi.org/10.1175/JCLI-D-23-0522.1, 2024.

Bishop, C. M. and Nasrabadi, N. M.: Pattern recognition and machine learning, vol. 4, Springer, 2006.

Bock, L. and Lauer, A.: Cloud properties and their projected changes in CMIP models with low to high climate sensitivity, Atmospheric Chemistry and Physics, 24, 1587–1605, https://doi.org/10.5194/acp-24-1587-2024, 2024.

Bordbar, M. H., Mohrholz, V., and Schmidt, M.: Low confidence in multi-decadal trends of wind-driven upwelling across the Benguela Upwelling System, Earth System Dynamics, 14, 1065–1080, https://doi.org/10.5194/esd-14-1065-2023, 2023.

Boucher, O., Servonnat, J., Albright, A. L., Aumont, O., Balkanski, Y., Bastrikov, V., Bekki, S., Bonnet, R., Bony, S., Bopp, L., et al.: Presentation and evaluation of the IPSL-CM6A-LR climate model, Journal of Advances in Modeling Earth Systems, 12, e2019MS002 010, https://doi.org/10.1029/2019MS002010, 2020.

Bretherton, C. S., Blossey, P. N., and Jones, C. R.: Mechanisms of marine low cloud sensitivity to idealized climate perturbations: A single-LES exploration extending the CGILS cases, Journal of Advances in Modeling Earth Systems, 5, 316–337, https://doi.org/10.1002/jame.20019, 2013.

Ceppi, P. and Nowack, P.: Observational evidence that cloud feedback amplifies global warming, Proceedings of the National Academy of Sciences, 118, e2026290 118, https://doi.org/10.1073/pnas.2026290118, 2021.

Ceppi, P., Wilson Kemsley, S., Andersen, H., Andrews, T., Kramer, R. J., Nowack, P., Wall, C. J., and Zelinka, M. D.: Emerging low-cloud feedback and adjustment in global satellite observations, EGUsphere, 2025, 1–24, https://doi.org/10.5194/acp-26-4153-2026, 2025.

Cermak, J.: Low clouds and fog along the South-Western African coast—Satellite-based retrieval and spatial patterns, Atmospheric Research, 116, 15–21, https://doi.org/10.1016/j.atmosres.2011.02.012, 2012.

Christensen, M. W., Carrió, G. G., Stephens, G. L., and Cotton, W. R.: Radiative Impacts of Free-Tropospheric Clouds on the Properties of Marine Stratocumulus, Journal of the Atmospheric Sciences, 70, 3102 – 3118, https://doi.org/10.1175/JAS-D-12-0287.1, 2013.

https://doi.org/10.5194/egusphere-2026-3242
Preprint. Discussion started: 25 June 2026

Dormann, C. F., Elith, J., Bacher, S., Buchmann, C., Carl, G., Carré, G., Marquéz, J. R. G., Gruber, B., Lafourcade, B., Leitão, P. J., et al.: Collinearity: a review of methods to deal with it and a simulation study evaluating their performance, Ecography, 36, 27–46, https://doi.org/10.1111/j.1600-0587.2012.07348.x, 2013.

Ebner, M., Miranda, T., and Roth-Nebelsick, A.: Efficient fog harvesting by Stipagrostis sabulicola (Namib dune bushman grass), Journal of arid environments, 75, 524–531, https://doi.org/10.1016/j.jaridenv.2011.01.004, 2011.

Eyring, V., Bony, S., Meehl, G. A., Senior, C. A., Stevens, B., Stouffer, R. J., and Taylor, K. E.: Overview of the Coupled Model Intercomparison Project Phase 6 (CMIP6) experimental design and organization, Geoscientific Model Development, 9, 1937–1958, https://doi.org/10.5194/gmd-9-1937-2016, 2016.

Fu, G., Xu, W., Yang, R., Li, J., and Zhao, C.: The distribution and trends of fog and haze in the North China Plain over the past 30 years, Atmospheric Chemistry and Physics, 14, 11 949–11 958, https://doi.org/10.5194/acp-14-11949-2014, 2014.

Gallego, D., García-Herrera, R., Tomety, F. S., Álvarez-Castro, M. C., and Peña-Ortiz, C.: Historical record of upwelling-favorable winds in Southern Benguela 1833–2014, npj Climate and Atmospheric Science, 8, 36, https://doi.org/10.1038/s41612-025-00925-0, 2025.

Gelaro, R., McCarty, W., Suárez, M. J., Todling, R., Molod, A., Takacs, L., Randles, C. A., Darmenov, A., Bosilovich, M. G., Reichle, R., Wargan, K., Coy, L., Cullather, R., Draper, C., Akella, S., Buchard, V., Conaty, A., da Silva, A. M., Gu, W., Kim, G.-K., Koster, R., Lucchesi, R., Merkova, D., Nielsen, J. E., Partyka, G., Pawson, S., Putman, W., Rienecker, M., Schubert, S. D., Sienkiewicz, M., and Zhao, B.: The Modern-Era Retrospective Analysis for Research and Applications, Version 2 (MERRA-2), Journal of Climate, 30, 5419 – 5454, https://doi.org/10.1175/JCLI-D-16-0758.1, 2017.

Global Modeling and Assimilation Office and Pawson, S.: MERRA-2 instM_3d_ana_Np: 3d, Monthly Mean, Instantaneous, Pressure-Level, Analysis, Analyzed Meteorological Fields V5.12.4, https://doi.org/10.5067/V92O8XZ30XBI, accessed: 2026-02-17, 2015a.

Global Modeling and Assimilation Office and Pawson, S.: MERRA-2 instM_2d_asm_Nx: 2d, Monthly Mean, Single-Level, Assimilation, Single-Level Diagnostics V5.12.4, https://doi.org/10.5067/5ESKGQTZG7FO, accessed: 2026-02-17, 2015b.

Global Modeling and Assimilation Office and Pawson, S.: MERRA-2 inst1_2d_asm_Nx: 2d, 3-Hourly, Instantaneous, Single-Level, Assimilation, Single-Level Diagnostics V5.12.4, https://doi.org/10.5067/3Z173KIE2TPD, accessed: 2026-02-17, 2015c.

Gray, E., Gilardoni, S., Baldocchi, D., McDonald, B. C., Facchini, M. C., and Goldstein, A. H.: Impact of air pollution controls on radiation fog frequency in the Central Valley of California, Journal of Geophysical Research: Atmospheres, 124, 5889–5905, https://doi.org/10.1029/2018JD029419, 2019.

Gregory, J. M.: Vertical heat transports in the ocean and their effect on time-dependent climate change, Climate Dynamics, 16, 501–515, https://doi.org/10.1007/s003820000059, 2000.

Gultepe, I., Tardif, R., Michaelides, S. C., Cermak, J., Bott, A., Bendix, J., Müller, M. D., Pagowski, M., Hansen, B., Ellrod, G., et al.: Fog research: A review of past achievements and future perspectives, Pure and applied geophysics, 164, 1121–1159, https://doi.org/10.1007/s00024-007-0211-x, 2007.

Haensler, A., Cermak, J., Hagemann, S., and Jacob, D.: Will the southern African west coast fog be affected by future climate change? Results of an initial fog projection using a regional climate model, Erdkunde, pp. 261–275, https://doi.org/10.3112/erdkunde.2011.03.04, 2011.

He, B., Bao, Q., Wang, X., Zhou, L., Wu, X., Liu, Y., Wu, G., Chen, K., He, S., Hu, W., et al.: CAS FGOALS-f3-L model datasets for CMIP6 historical atmospheric model intercomparison project simulation, Advances in Atmospheric Sciences, 36, 771–778, https://doi.org/10.1007/s00376-019-9027-8, 2019.

https://doi.org/10.5194/egusphere-2026-3242
Preprint. Discussion started: 25 June 2026

Hersbach, H., Bell, B., Berrisford, P., Hirahara, S., Horányi, A., Muñoz-Sabater, J., Nicolas, J., Peubey, C., Radu, R., Schepers, D., Simmons, A., Soci, C., Abdalla, S., Abellan, X., Balsamo, G., Bechtold, P., Biavati, G., Bidlot, J., Bonavita, M., De Chiara, G., Dahlgren, P., Dee, D., Diamantakis, M., Dragani, R., Flemming, J., Forbes, R., Fuentes, M., Geer, A., Haimberger, L., Healy, S., Hogan, R. J., Hólm, E., Janisková, M., Keeley, S., Laloyaux, P., Lopez, P., Lupu, C., Radnoti, G., de Rosnay, P., Rozum, I., Vamborg, F., Villaume, S., and Thépaut, J.-N.: The ERA5 global reanalysis, Quarterly Journal of the Royal Meteorological Society, 146, 1999–2049, https://doi.org/10.1002/qj.3803, 2020.

Hipler, V., Andersen, H., Spirig, R., Vogt, R., Piketh, S., Adler, B., and Cermak, J.: Synoptic and regional-scale meteorological controls of stratus altitude in the Namib Desert, EGUsphere, pp. 1–22, https://doi.org/10.5194/egusphere-2025-5816, 2026.

Hoerl, A. E. and Kennard, R. W.: Ridge regression: Biased estimation for nonorthogonal problems, Technometrics, 12, 55–67, https://doi.org/10.1080/00401706.1970.10488634, 1970.

Huang, B., Liu, C., Banzon, V., Freeman, E., Graham, G., Hankins, B., Smith, T., and Zhang, H.-M.: Improvements of the daily optimum interpolation sea surface temperature (DOISST) version 2.1, Journal of Climate, 34, 2923–2939, https://doi.org/10.1175/JCLI-D-20-0166.1, 2021.

Huber, M. B. and Zanna, L.: Drivers of uncertainty in simulated ocean circulation and heat uptake, Geophysical Research Letters, 44, 1402–1413, https://doi.org/10.1002/2016GL071587, 2017.

Iturbide, M., Gutiérrez, J. M., Alves, L. M., Bedia, J., Cerezo-Mota, R., Cimadevilla, E., Cofiño, A. S., Di Luca, A., Faria, S. H., Gorodetskaya, I. V., et al.: An update of IPCC climate reference regions for subcontinental analysis of climate model data: definition and aggregated datasets, Earth System Science Data, 12, 2959–2970, https://doi.org/10.5194/essd-12-2959-2020, 2020.

Jacob, D.: A note to the simulation of the annual and inter-annual variability of the water budget over the Baltic Sea drainage basin, Meteorology and Atmospheric Physics, 77, 61–73, https://doi.org/10.1007/s007030170017, 2001.

Klein, S. A., Hall, A., Norris, J. R., and Pincus, R.: Low-cloud feedbacks from cloud-controlling factors: A review, Surveys in Geophysics, pp. 135–157, https://doi.org/10.1007/s10712-017-9433-3, 2018.

Klemm, O. and Lin, N.-H.: What causes observed fog trends: Air quality or climate change?, Aerosol and Air Quality Research, 16, 1131–1142, https://doi.org/10.4209/aaqr.2015.05.0353, 2016.

Knutti, R., Masson, D., and Gettelman, A.: Climate model genealogy: Generation CMIP5 and how we got there, Geophysical Research Letters, 40, 1194–1199, https://doi.org/10.1002/grl.50256, 2013.

Lahiri, S. N.: Resampling methods for dependent data, Springer Science & Business Media, https://doi.org/10.1007/978-1-4757-3803-2, 2003.

Lancaster, J., Lancaster, N., and Seely, M. K.: Climate of the central Namib Desert, Madoqua, 1984, 5–61, https://doi.org/https://hdl.handle.net/10520/AJA10115498_484, 1984.

Li, Y., Wang, L., Diersing, C. J., Qiao, N., Liu, Y., Maggs-Kölling, G., and Marais, E.: El Niño intensified fog formation in the Namib Desert, Earth's Future, 13, e2024EF005 725, https://doi.org/10.1029/2024EF005725, 2025.

Loeb, N. G. and Doelling, D. R.: CERES energy balanced and filled (EBAF) from afternoon-only satellite orbits, Remote Sensing, 12, 1280, https://doi.org/10.3390/rs12081280, 2020.

Loeb, N. G., Doelling, D. R., Wang, H., Su, W., Nguyen, C., Corbett, J. G., Liang, L., Mitrescu, C., Rose, F. G., and Kato, S.: Clouds and the earth's radiant energy system (CERES) energy balanced and filled (EBAF) top-of-atmosphere (TOA) edition-4.0 data product, Journal of climate, 31, 895–918, https://doi.org/10.1175/JCLI-D-17-0208.1, 2018.

https://doi.org/10.5194/egusphere-2026-3242
Preprint. Discussion started: 25 June 2026

Louw, G. N. and Holm, E.: Physiological, morphological and behavioural adaptations of the ultrapsammophilous, Namib Desert lizard Aporosaura anchietae (Bocage), Madoqua, 1, 67–85, 1972.

Malik, D., Andersen, H., Cermak, J., Vogt, R., and Adler, B.: Cloud base height determines fog occurrence patterns in the Namib Desert, Atmospheric Chemistry and Physics, 26, 681–701, https://doi.org/10.5194/acp-26-681-2026, 2026.

Maraun, D.: Bias correcting climate change simulations-a critical review, Current Climate Change Reports, 2, 211–220, https://doi.org/10.1007/S40641-016-0050-X, 2016.

Mass, A., Andersen, H., Cermak, J., Formenti, P., Pauli, E., and Quinting, J.: A satellite-based analysis of semi-direct effects of biomass burning aerosols on fog and low-cloud dissipation in the Namib Desert, Atmospheric Chemistry and Physics, 25, 491–510, https://doi.org/10.5194/acp-25-491-2025, 2025.

Mass, A., Andersen, H., and Cermak, J.: Coastal upwelling and tropical warm water intrusions are key drivers of interannual fog variability along the southwestern African coast, EGUsphere, 2026, 1–29, https://doi.org/10.5194/egusphere-2026-1208, 2026.

Masson-Delmotte, V., Zhai, P., Pirani, A., Connors, S. L., Péan, C., Berger, S., Caud, N., Chen, Y., Goldfarb, L., Gomis, M. I., Huang, M., Leitzell, K., Lonnoy, E., Matthews, J. B. R., Maycock, T. K., Waterfield, T., Yelekçi, O., Yu, R., and Zhou, B., eds.: Climate Change 2021: The Physical Science Basis, Cambridge University Press, Cambridge, United Kingdom and New York, NY, USA, https://doi.org/10.1017/9781009157896, 2021.

Maúre, G., Pinto, I., Ndebele-Murisa, M., Muthige, M., Lennard, C., Nikulin, G., Dosio, A., and Meque, A.: The southern African climate under 1.5°C and 2°C of global warming as simulated by CORDEX regional climate models, Environmental Research Letters, 13, 065 002, https://doi.org/10.1088/1748-9326/aab190, 2018.

Maurer, M., Klemm, O., Lokys, H. L., and Lin, N.-H.: Trends of fog and visibility in Taiwan: climate change or air quality improvement?, Aerosol and Air Quality Research, 19, 896–910, https://doi.org/10.4209/aaqr.2018.04.0152, 2019.

Mauritsen, T., Bader, J., Becker, T., Behrens, J., Bittner, M., Brokopf, R., Brovkin, V., Claussen, M., Crueger, T., Esch, M., et al.: Developments in the MPI-M Earth System Model version 1.2 (MPI-ESM1.2) and its response to increasing CO_2, Journal of Advances in Modeling Earth Systems, 11, 998–1038, https://doi.org/10.1029/2018MS001400, 2019.

Meehl, G. A., Senior, C. A., Eyring, V., Flato, G., Lamarque, J.-F., Stouffer, R. J., Taylor, K. E., and Schlund, M.: Context for interpreting equilibrium climate sensitivity and transient climate response from the CMIP6 Earth system models, Science Advances, 6, eaba1981, https://doi.org/10.1126/sciadv.aba1981, 2020.

Merrifield, A. L., Brunner, L., Lorenz, R., Humphrey, V., and Knutti, R.: Climate model Selection by Independence, Performance, and Spread (ClimSIPS v1. 0.1) for regional applications, Geoscientific Model Development, 16, 4715–4747, https://doi.org/10.5194/gmd-16-4715-2023, 2023.

Mitchell, D., Henschel, J. R., Hetem, R. S., Wassenaar, T. D., Strauss, W. M., Hanrahan, S. A., and Seely, M. K.: Fog and fauna of the Namib Desert: past and future, Ecosphere, 11, e02 996, https://doi.org/10.1002/ecs2.2996, 2020.

Munday, C., Washington, R., Engelstaedter, S., Zilli, M., Harbord, S., Knight, C., Attwood, K., and Hart, N.: Southern African Climate Change: Processes, Models, and Projections, Wiley Interdisciplinary Reviews: Climate Change, 16, e70 025, https://doi.org/10.1002/wcc.70025, 2025.

Myers, T. A. and Norris, J. R.: Reducing the uncertainty in subtropical cloud feedback, Geophysical Research Letters, 43, 2144–2148, https://doi.org/10.1002/2015GL067416, 2016.

Myers, T. A., Scott, R. C., Zelinka, M. D., Klein, S. A., Norris, J. R., and Caldwell, P. M.: Observational constraints on low cloud feedback reduce uncertainty of climate sensitivity, Nature Climate Change, 11, 501–507, https://doi.org/10.1038/s41558-021-01039-0, 2021.

https://doi.org/10.5194/egusphere-2026-3242
Preprint. Discussion started: 25 June 2026

Olivier, J. and Stockton, P.: The influence of upwelling extent upon fog incidence at Lüderitz, southern Africa, International Journal of Climatology, 9, 69–75, https://doi.org/10.1002/joc.3370090106, 1989.

O'Neill, B. C., Kriegler, E., Ebi, K. L., Kemp-Benedict, E., Riahi, K., Rothman, D. S., van Ruijven, B. J., van Vuuren, D. P., Birkmann, J., Kok, K., Levy, M., and Solecki, W.: The roads ahead: Narratives for shared socioeconomic pathways describing world futures in the 21st century, Global Environmental Change, 42, 169–180, https://doi.org/10.1016/j.gloenvcha.2015.01.004, 2017.

Rohde, R. F., Hoffman, M. T., Durbach, I., Venter, Z., and Jack, S.: Vegetation and climate change in the Pro-Namib and Namib Desert based on repeat photography: Insights into climate trends, Journal of Arid Environments, 165, 119–131, https://doi.org/10.1016/j.jaridenv.2019.01.007, 2019.

Schmetz, J., Pili, P., Tjemkes, S., Just, D., Kerkmann, J., Rota, S., and Ratier, A.: An introduction to Meteosat second generation (MSG), Bulletin of the American Meteorological Society, 83, 977–992, https://doi.org/10.1175/1520-0477(2002)083<0977:AITMSG>2.3.CO;2, 2002.

Scott, R. C., Myers, T. A., Norris, J. R., Zelinka, M. D., Klein, S. A., Sun, M., and Doelling, D. R.: Observed Sensitivity of Low-Cloud Radiative Effects to Meteorological Perturbations over the Global Oceans, Journal of Climate, 33, 7717 – 7734, https://doi.org/10.1175/JCLI-D-19-1028.1, 2020.

Seely, M. K. and Henschel, J. R.: The climatology of Namib fog, in: Proceedings of the First International Conference on Fog and Fog Collection, pp. 353–356, 1998.

Sellar, A. A., Jones, C. G., Mulcahy, J. P., Tang, Y., Yool, A., Wiltshire, A., O'connor, F. M., Stringer, M., Hill, R., Palmieri, J., et al.: UKESM1: Description and evaluation of the UK Earth System Model, Journal of Advances in Modeling Earth Systems, 11, 4513–4558, https://doi.org/10.1029/2019MS001739, 2019.

Simpson, I. R., Shaw, T. A., Ceppi, P., Clement, A. C., Fischer, E., Grise, K. M., Pendergrass, A. G., Screen, J. A., Wills, R. C., Woollings, T., et al.: Confronting earth system model trends with observations, Science advances, 11, eadt8035, https://doi.org/10.1126/sciadv.adt8035, 2025.

Spirig, R., Vogt, R., Larsen, J. A., Feigenwinter, C., Wicki, A., Franceschi, J., Parlow, E., Adler, B., Kalthoff, N., Cermak, J., Andersen, H., Fuchs, J., Bott, A., Hacker, M., Wagner, N., Maggs-Kölling, G., Wassenaar, T., and Seely, M.: Probing the fog life cycles in the Namib Desert, Bulletin of the American Meteorological Society, 100, 2491–2507, https://doi.org/10.1175/BAMS-D-18-0142.1, 2019.

Tatro, T. and Zuidema, P.: More biomass burning aerosol is being advected westward over the southern tropical Atlantic since 2003, Science of The Total Environment, 965, 178 506, https://doi.org/10.1016/j.scitotenv.2025.178506, 2025.

Taylor, K. E., Stouffer, R. J., and Meehl, G. A.: An overview of CMIP5 and the experiment design, Bulletin of the American meteorological Society, 93, 485–498, https://doi.org/10.1175/BAMS-D-11-00094.1, 2012.

Teutschbein, C. and Seibert, J.: Bias correction of regional climate model simulations for hydrological climate-change impact studies: Review and evaluation of different methods, Journal of hydrology, 456, 12–29, https://doi.org/10.1016/j.jhydrol.2012.05.052, 2012.

Vautard, R., Yiou, P., and Van Oldenborgh, G. J.: Decline of fog, mist and haze in Europe over the past 30 years, Nature Geoscience, 2, 115–119, https://doi.org/10.1038/ngeo414, 2009.

Voldoire, A., Saint-Martin, D., Sénési, S., Decharme, B., Alias, A., Chevallier, M., Colin, J., Guérémy, J.-F., Michou, M., Moine, M.-P., et al.: Evaluation of CMIP6 deck experiments with CNRM-CM6-1, Journal of Advances in Modeling Earth Systems, 11, 2177–2213, https://doi.org/10.1029/2019MS001683, 2019.

Wang, D., Gouhier, T. C., Menge, B. A., and Ganguly, A. R.: Intensification and spatial homogenization of coastal upwelling under climate change, Nature, 518, 390–394, https://doi.org/10.1038/nature14235, 2015.

https://doi.org/10.5194/egusphere-2026-3242
Preprint. Discussion started: 25 June 2026

Wang, L., Kaseke, K. F., Ravi, S., Jiao, W., Mushi, R., Shuuya, T., and Maggs-Kölling, G.: Convergent vegetation fog and dew water use in the Namib Desert, Ecohydrology, 12, e2130, https://doi.org/10.1002/eco.2130, 2019.

Warren-Rhodes, K. A., McKay, C. P., Boyle, L. N., Wing, M. R., Kiekebusch, E. M., Cowan, D. A., Stomeo, F., Pointing, S. B., Kaseke, K. F., Eckardt, F., Henschel, J. R., Anisfeld, A., Seely, M., and Rhodes., K. L.: Physical ecology of hypolithic communities in the central Namib Desert: the role of fog, rain, rock habitat, and light, Journal of Geophysical Research: Biogeosciences, 118, 1451–1460, https://doi.org/10.1002/jgrg.20117, 2013.

Wilson Kemsley, S., Ceppi, P., Andersen, H., Cermak, J., Stier, P., and Nowack, P.: A systematic evaluation of high-cloud controlling factors, Atmospheric Chemistry and Physics, 24, 8295–8316, https://doi.org/10.5194/acp-24-8295-2024, 2024.

Witiw, M. and LaDochy, S.: Trends in fog frequencies in the Los Angeles Basin, Atmospheric Research, 87, 293–300, https://doi.org/10.1016/j.atmosres.2007.11.010, 2008.

Wood, R. and Bretherton, C. S.: On the relationship between stratiform low cloud cover and lower-tropospheric stability, Journal of climate, 19, 6425–6432, https://doi.org/10.1175/JCLI3988.1, 2006.

Wu, M., Su, H., and Neelin, J. D.: Multi-objective observational constraint of tropical Atlantic and Pacific low-cloud variability narrows uncertainty in cloud feedback, Nature Communications, 16, 218, https://doi.org/10.1038/s41467-024-53985-w, 2025.

Zelinka, M. D., Myers, T. A., McCoy, D. T., Po-Chedley, S., Caldwell, P. M., Ceppi, P., Klein, S. A., and Taylor, K. E.: Causes of higher climate sensitivity in CMIP6 models, Geophysical Research Letters, 47, e2019GL085 782, https://doi.org/10.1029/2019GL085782, 2020.

Zuidema, P., Chang, P., Medeiros, B., Kirtman, B. P., Mechoso, R., Schneider, E. K., Toniazzo, T., Richter, I., Small, R. J., Bellomo, K., et al.: Challenges and prospects for reducing coupled climate model SST biases in the eastern tropical Atlantic and Pacific oceans: The US CLIVAR Eastern Tropical Oceans Synthesis Working Group, Bulletin of the American Meteorological Society, 97, 2305–2328, https://doi.org/10.1175/BAMS-D-15-00274.1, 2016.